Riset Geologi dan Pertambangan
(Geology and Mining Research)

RESEARCH ARTICLE
OPEN ACCESS

Riset Geologi dan Pertambangan (2025) Vol. 35, No. 2, 131–148
DOI: 10.55981/risetgeotam.2025.1457

***Keywords:***
Landslide
Debris flow
Non-Newtonian flow
Smoothed particle hydrodynamics
Computational fluid dynamics

***Corresponding author:***
Indra Andra Dinata
indraandradinata@gmail.com

***Article history:***
Received: 14 August 2025
Revised: 03 October 2025
Accepted: 05 October 2025

***Author Contributions:***
Conceptualization: IAD
Data curation: IAD
Formal analysis: IAD
Funding acquisition: IAS
Investigation: IAD
Methodology: IAD
Supervision: IAS, PS, LMH
Visualization: IAD
Writing – original draft: IAD
Writing – review & editing: IAD

***Citation:***
Dinata, I.A., Sadisun, I.A., Soemintadiredja, P., Hutasoit, L.M., 2025. Deterministic Modeling of Pasir Panjang Debris Flow Using Smoothed Particle Hydrodynamics (SPH). *Riset Geologi dan Pertambangan, 35 (2)*, 131–148, doi: 10.55981/risetgeotam.2025.1457



# Deterministic Modeling of Pasir Panjang Debris Flow Using Smoothed Particle Hydrodynamics (SPH)

Indra Andra Dinata[1], Imam Achmad Sadisun[2], Prihadi Soemintadiredja[3], Lambok M Hutasoit[2]

[1]Doctoral Program of Geological Engineering, Faculty of Earth Sciences and Technology, Bandung Institute of Technology (ITB), Bandung, West Java 40132, Indonesia
[2]Applied Geology Research Group, Faculty of Earth Sciences and Technology, Bandung Institute of Technology (ITB), Bandung, West Java 40132, Indonesia
[3]Petrology, Volcanology, and Geochemistry Research Group, Faculty of Earth Sciences and Technology, Bandung Institute of Technology (ITB), Bandung, West Java 40132, Indonesia

## Abstract

The debris flow can be modeled as non-Newtonian flow using physical and mathematical modeling methods based on rheological property measurements and movement parameters. The numerical simulation in this research used smoothed particle hydrodynamics (SPH) to solve the momentum and energy equations. The debris flow modeled in this research is located in the Bentarsari Basin, which is surrounded by hills composed of volcanic breccia from the Kumbang Formation (Tpk) and tends to be more susceptible to landslides and may become debris flows. The results of the numerical simulation begin with the collapse of the natural dam and become debris flow with 8.8 m maximum thickness. The debris flow destroyed the bridge in the 40s with 100 kPa pressure. A speed of 6 m/s was reached at 120 s. A small hill in the deposition area was hit by debris flow at 130 s, causing 18 casualties. The debris flow enters the deposition area at 150 s. The debris flow average velocity shows relatively transverse pattern (1-126 s), constant pattern (126-289 s), and random pattern (after 289 s). The debris flow average pressure shows steep negative gradient pattern (1-47 s) and a relatively flat pattern (after 47 s). The average debris flow thickness shows a steep negative gradient pattern (1-13 s) and a gentle negative gradient pattern (after 13 s). The results of debris flow modeling using SPH can simulate the debris flow segregation process, which usually cannot be captured by conventional debris flow modeling software.

## 1. Introduction

Indonesia is a country highly prone to landslides. These events frequently occur in areas with relatively steep slopes (Ahmid et al., 2023; Dzaki et al., 2024), intense weathering processes, and high rainfall. Landslides that contain a mixture of solid and liquid materials can transform into debris flows. Several landslides are followed by debris flows, such as Karangkobar debris flow occurred in 2014 in Banjarnegara Regency, Central Java Province which claimed more than 100 lives (Sadisun et al., 2018).

Debris flow can be modeled as non-Newtonian flow using physical and mathematical modeling methods based on rheological property measurements and movement parameters.

Several software packages have been used for debris flow modeling by previous researchers, employing different analysis methods such as Debris2D (Hsu and Liu, 2019), Flo-2D (Agostino and Tecca, 2006), Kanako 2D (Sadisun et al., 2019), RAMMS (Hussin et al., 2012), Flow-R (Putra et al., 2022), and TRIGRS (Alvioli and Baum, 2016). These software packages offered useful features for debris flow modeling; however, some approaches still lack the ability to simulate the separation process of debris material (Jakob, 2010). The separation process can be addressed by refining the model using the discrete element method (DEM). The DEM model is incorporated into the smoothed particle hydrodynamics (SPH) model applied in this research.

The Bentarsari Basin, Brebes Regency, Central Java Province, Indonesia was chosen for this study because debris flow events have occurred there 19 times up to 2025. One notable debris flow in this basin was the debris flow in Pasir Panjang Village, on February 22, 2018, which claimed 18 lives. Therefore, this study aims to investigate the mechanism of the debris flow event for February 22, 2018 in Pasir Panjang Village, with the goal of informing mitigation strategies for potential future debris flows in the Bentarsari Basin.

## 2. Materials and Methods

### Materials

The main materials used in modeling the debris flow were moderately to highly weathered volcanic breccia (Figure 1) and completely weathered volcanic breccia to residual soil. Both materials were derived from the Kumbang Formation (Tpk) (Kastowo, 1975), which is more susceptible to landslides and may evolve into debris flows. The moderately to highly weathered volcanic breccia is grayish brown in color and contains pebble- to boulder-sized (>4 mm) andesite fragments that can be picked up by hand and are relatively weak. This unit was observed along the riverbed, within the flow track, and in the source area.

The completely weathered volcanic breccia to residual soil, derived from volcanic breccia, is characterized by a brown to grayish-brown color and a fine- to medium-sand grain size (0.125–0.5 mm). In some locations, andesite fragments are still present. This unit has a thickness of approximately 3–15 m and dominates the debris-flow material. The material contains abundant organic matter, mainly in the form of plant remains, and is distributed along the riverbank. Based on laboratory data, the material's plasticity is classified as medium to high, with a bulk density of 1.82–1.86 g/cm$^3$, natural water content of 9.22–11.86%, cohesion of 0.20–0.23 kg/cm$^2$, and an internal friction angle of 23.04–27.65°, indicating that it is classified as clay soil.

In addition to the material properties, hydrological inputs play a crucial role in determining the behavior of debris flows in the SPH modeling. The supply hydrograph, which represent the inflow condition for simulation, affects the flow viscosity and thereby determines the rheological conditions of the debris flow. In this study, the supply hydrograph was approximated by combining the surface water flow rate and rainfall intensity. Based on the results of the Cipagurugan River flow rate measurements, the river discharge ranges from 0.8 m3/s in the northern section to 1.4 m$^3$/s in the southern (foot slope) area. The rainfall intensity value was obtained from the PK.5c Dukuhjeruk rainfall station, which is the closest distance with research area (Table 1).


**Figure 1. a**) Outcrops of moderately to highly weathered volcanic breccia on the riverbed; **b**) completely weathered volcanic breccia to residual soil on the source area.

**Table 1.** PK.5c Dukuhjeruk 2009-2015 Monthly rainfall data

| Year | Jan | Feb | Mar | Apr | May | Jun | Jul | Aug | Sep | Oct | Nov | Dec |
|---|---|---|---|---|---|---|---|---|---|---|---|---|
| 2009 | 266 | 287 | 195 | 190 | 207 | 109 | 19 | 0 | 0 | 22 | 262 | 22 |
| 2010 | 391 | 295 | 493 | 299 | 302 | 181 | 35 | 100 | 155 | 90 | 130 | 283 |
| 2011 | 81 | 459 | 481 | 171 | 208 | 37 | 43 | 0 | 0 | 70 | 245 | 475 |
| 2012 | 223 | 434 | 269 | 23 | 131 | 15 | 0 | 0 | 0 | 34 | 169 | 291 |
| 2013 | 415 | 198 | 193 | 197 | 148 | 289 | 91 | 0 | 0 | 34 | 131 | 202 |
| 2014 | 233 | 286 | 256 | 170 | 149 | 83 | 65 | 7 | 0 | 7 | 125 | 289 |
| 2015 | 227 | 143 | 177 | 152 | 119 | 9 | 8 | 0 | 0 | 0 | 49 | 197 |
| Max | 391 | 459 | 493 | 299 | 302 | 181 | 43 | 100 | 155 | 90 | 262 | 475 |
| Average | 240 | 369 | 360 | 171 | 212 | 86 | 24 | 25 | 39 | 54 | 202 | 268 |
| Min | 81 | 287 | 195 | 23 | 131 | 15 | 0 | 0 | 0 | 22 | 130 | 22 |

## Debris Flow as Non-Newtonian Flow

Debris flows typically begin as flooding on steep mountain slopes and transport large amounts of suspended and bedload sediments. When the sediment concentration increases beyond a certain threshold, the flow changes into a thick mass consisting of water, soil, sand, gravel, rocks, and logs mixed together that moves through valley channels in a lava-like manner (Jakob and Hungr 2005). Debris flows are also defined as masses of solid material, water, and air that behave as a liquid flow. They can be characterized as non-Newtonian flow. A debris flows consists of three main parts: the source area, the flow track, and the depositional area (Blijenberg, 2007).

Debris flows can be classified into two types: hillslope and channelized debris flows (Nettleton et al., 2005). The front (or head) of a debris flow is typically higher than the remainder and contains large, moving boulders, followed by a more turbulent, mud-rich fluid with high suspended-sediment viscosity (Song et al., 2018). This fluid phase continues until the arrival of the next surge or until debris-flow activity ceases (Pierson, 1980; Choi et al., 2015; Choi et al., 2016). Debris flows are highly erosive as they move along the flow track (Federico and Cesali, 2019). Along the flow path, the density of the debris flow can be up to twice that of the accompanying fluid, and the shear stress on the streambed can increase by up to sixfold (Janda et al., 1981). This increase in shear stress is often caused by the sudden loading of landslide material in the source area (Berger et al., 2011).

## Governing Equation

The numerical simulations in this study were conducted using the smoothed particle hydrodynamics (SPH) method, which is derived from the Monaghan formulation (Monaghan, 1992). The SPH method does not require a fixed computational grid; instead, it uses analytical differentials to interpolate governing equations. The momentum and energy equations are expressed as systems of ordinary differential equations (ODEs). The governing equations for the flow consist of the continuity and momentum equations in Lagrangian form. The Lo and Shao (2002) formulation was applied under laminar flow conditions to compute the corresponding viscous dissipation term (Equation 1).

$$v_0 \nabla^2 v_a = \sum_{b \in P} m_b \frac{4 v_0 r_{ab} . \nabla W_{ab}}{(\rho_a + \rho_b)(r_{ab}^2 + \eta^2)} v_{ab} . \quad (1)$$

where:
$v_0$ – kinematic viscosity of fluid (Pa.s)
$v$ – velocity (m/s)
$r$ – fluid particle radius (mm)
$a$ and $b$ – material identity
$m$ – mass (kg)
$W$ – compact support of kernel
$\rho$ – density (kg/m$^3$)
$\eta$ – value to avoid singularity (0.1 of kernel smoothing distance)

The turbulent and intermediate flow regimes can be described by artificial viscosity in the momentum equation, so the vibrations/oscillations of the flow can be stabilized in the SPH (Equation 2).

$$\frac{dv}{dt}\Big|_{a\in F} = -\sum_{b\in P} m_b \left(\frac{P_a + P_b}{\rho_a \rho_b} + \Pi_{ab}\right) \nabla W_{ab} + g \quad (2)$$

where:
$d$ – material derivatives
$F$ – force (N)
$\Pi$ – artificial viscosity (Pa.s)
$g$ – gravitational force (m/s$^2$)

The density and pressure used in the SPH formulation are combined with an equation of state (EOS), allowing for low compressibility in the fluid based on the numerical speed of sound (Monaghan, 1994). Therefore, the numerical speed of sound was chosen based on the typical length scale and time scale of the domain that allows a density variation of 1% and results in a Mach number $Ma \approx 0.1$, with $cs = 10\|\mathbf{v}\|max$. This restriction allows for larger time scales in explicit time integration (Equation 3).

$$P = \frac{c_s^2 \rho_0}{\gamma'} \left[\left(\frac{\rho}{\rho_0}\right)^{\gamma'} - 1\right] \quad (3)$$

where:
$P$ – pressure (kpa)
$c_s$ – numerical speed of sound ($\sqrt{\partial P/\partial \rho}$)
$\gamma'$ – damping coefficient
$\rho_0$ – initial density (kg/m$^3$)

The calculation process in each given time step uses two explicit time integration schemes. Equation 4 is integrated in time using a simple Verlet computation-based scheme and a symplectic Verlet position scheme, where $R_a$ is the derivative of density by time.

$$\frac{dv_a}{dt} = F_a;\ \frac{d\rho_a}{dt} = R_a;\ \frac{dr_a}{dt} = V_a \quad (4)$$

One of the most interesting capabilities of the SPH model is the simulation of solid materials driven by fluids. The application of this function to SPH produces the motion of a floating structure which considers interactions with fluid particles and uses the resulting forces to move the solid material. The total force on each floating solid material particle is calculated as a sum of the contributions from all surrounding fluid particles. The calculations can be integrated over time to obtain the values of v and Ω at the start of calculation at the next time step (Equation 5). The fluid particle assumed has granular shape while the solid particle assumed as rigid material and also has granular shape, allowing the fundamental equations of solid dynamics to be solved to obtain the motion (Canelas et al., 2017). Each solid material particle will move with a velocity $v_k$ and shown to conserve linear and angular momentum (Monaghan et al., 2003).

$$v_k = v + \Omega\,(r_k - R_0) \quad (5)$$

where:
$v_k$ – velocity of solid material particle (m/s)
$r_k$ – solid particle radius
Ω – angular velocity (rad/s)
$R_0$ – center of mass

The process to modeling the solid and liquid phases simultaneously can be assisted by the Herschel-Bulkley-Papanastasiou (HBP) model (Papanastasiou, 1987; Mitsoulis, 2007). The HBP approach allows modeling of various viscoplastic materials, including debris flow. In addition, the non-Newtonian HBP model can be used to simulate shear-thinning or thickening materials without yield strength. The Papanastasiou parameter controls the stress change with a finite value for small shear rates in areas where stress changes are expected, and linear behaviour in areas where stress changes occur (Morris et al., 1997; Fourtakas and Rogers, 2016).

Forces arise whenever a solid particle interacts with another particle (Jiang and Zhao 2015). These interaction forces are decomposed into $F_n$ (normal force) and $F_t$ (tangential force). Both of these forces include the effect of viscous dissipation. This is because the two interacting objects experience deformation between perfectly inelastic and perfectly elastic as measured by the normal coefficient of restitution in discrete element method (DEM) model (Figure 2). The total force generated after the collision is separated into two forces, namely $F^r$ (repulsive force) and $F^d$ (damping force). The equations for the repulsive force and the damping force generated after the interaction can be seen in Equations 6 and 7. The repulsive force arises from the elastic deformation caused by the particle collision. The damping force comes from the viscous dissipation of energy during deformation.

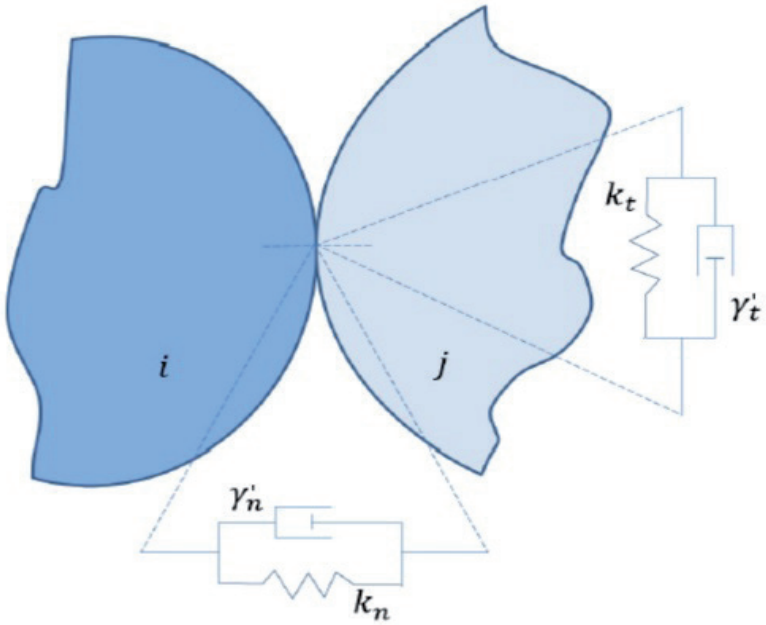


**Figure 2.** Interaction scheme between particles with viscoelastic DEM mechanism (Fourtakas and Rogers 2016).

$$F_{n,ij} = F_n^r + F_n^d = k_{n,ij}\delta_{ij}^{3/2}e_{ij}^n - \gamma'_{n,ij}\delta_{ij}^{1/2}\dot{\delta}_{ij}e_{ij}^n \quad (6)$$

$$F_{t,ij} = F_t^r + F_t^d = k_{t,ij}\delta_{ij}^t e_{ij}^t - \gamma'_{t,ij}\delta_{ij}^t\dot{\delta}_{ij}e_{ij}^t \quad (7)$$

where:
$F_n$ – normal force (N)
$F_t$ – tangential force (N)
$F^r$ – repulsive force (N)
$F^d$ – damping force (N)
$k$ – stiffness coefficient
$i$ and $j$ – tensor coordinate direction with Einstein notation
$\gamma'$ – damping coefficient

## 3. Implementation

Figure 3 shows the processing time with a 48-hour time limit. Processing time was compared with the number of particles modeled for each software type. The number of particles was limited by the hardware's modeling capability for 48 hours. The fastest modeling hardware was the NVIDIA Tesla V100 GPU, which was capable of modeling 80 million particles within a processing time of 47 hours (Dominguez et al., 2021). The second-fastest hardware was the NVIDIA GeForce RTX 2080Ti, which modeled 56 million particles in 36 hours.

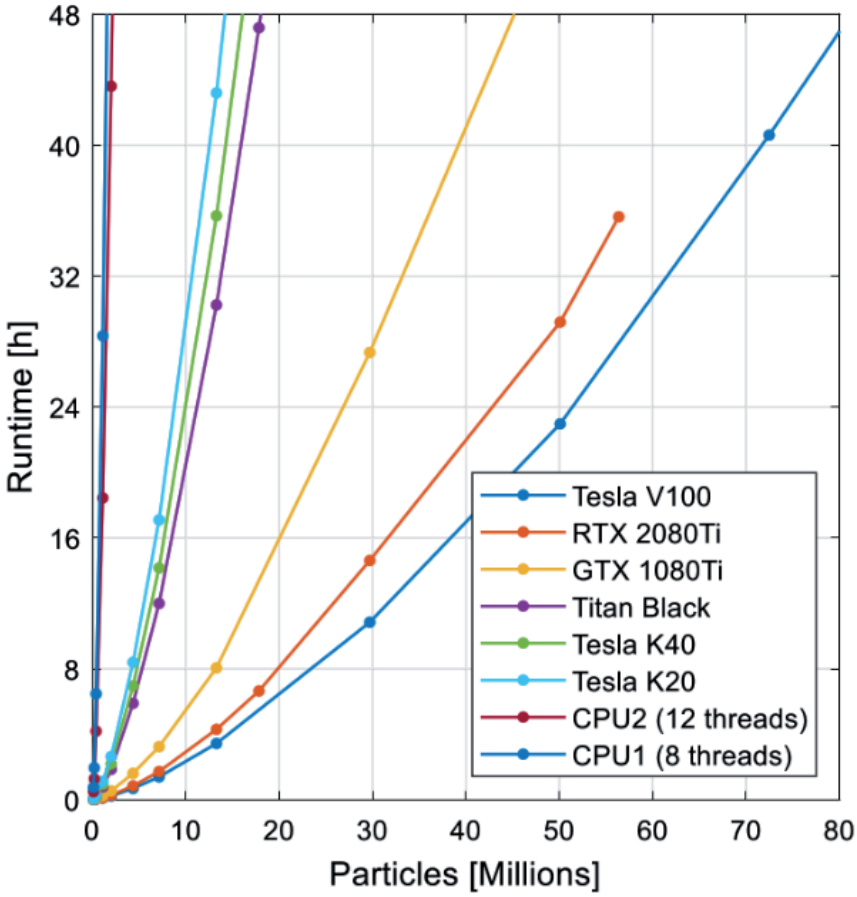


**Figure 3.** Particle processing time in DualSPHysics on different hardware types (Dominguez et al., 2021).

The number of base particles used in this research was approximately 1.5 million. The debris flow modeling time was conducted for 800 seconds with a 1-second time step between calculations; therefore, the total number of particles modeled was about 1.2 billion. Based on the findings of Domínguez et al. (2021), using the fastest available software, the processing time required would be approximately 705 hours (about one month) for each debris-flow scenario. To reduce the processing time, the computational hardware was upgraded. This study used an NVIDIA GeForce RTX 4090 GPU, which required only 36 hours of processing time. Hardware performance increases with model complexity, as a minimum number of particles is required to utilize the hardware efficiently and optimally. Once the hardware reaches its execution limit, performance no longer improves as the number of particles increases.

The drawbacks of the SPH model include its explicit nature, which may restrict the size of the modeling domain, and the fact that extended frictional contacts are either computationally expensive or inaccurately reproduced. Consequently, low-resolution simulations can introduce artificial geometric inaccuracies due to the representation of material as granular-shaped particles. Considering these limitations, and given its simplicity and computational efficiency, the SPH applications in this study were limited to debris-flow modeling from the source area to the depositional area at a 1:3,000 scale. To ensure that the governing equations could incorporate all relevant data and be implemented within the SPH framework, a well-organized workflow was developed, as illustrated in Figure 4.

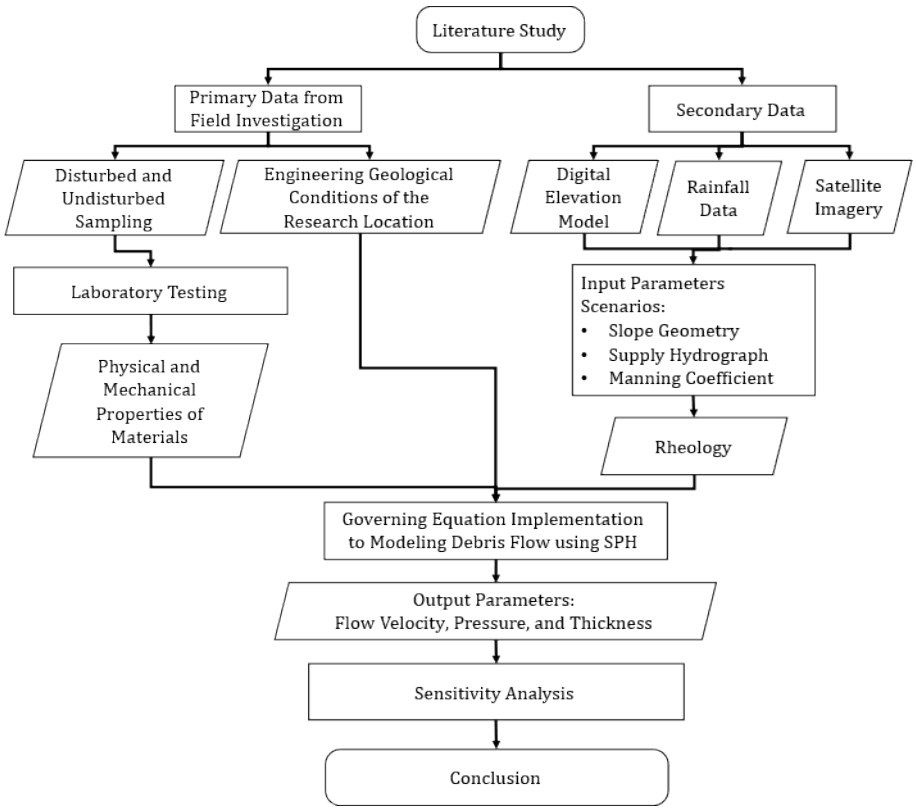


**Figure 4.** Workflow of debris flow modeling with SPH.

## 4. Parameters

The landslide in the source area has a circular sliding surface (Figure 5). The landslide measures approximately 200 m in length, 100 m in width, and 30 m in main scarp height, and includes several minor scarps. The volume of the landslide material was calculated using a half-elliptical approximation, resulting in a volume of approximately 348,889 $m^3$. The viscosity condition suitable for debris-flow initiation was approximated by concentration, with a value of 0.3 (Sadisun et al., 2019). The landslide material temporarily blocked the Cipagurugan River, forming a natural dam that persisted for five days (18–22 February 2018). The accumulation of upstream water caused the landslide material to exceed its yield stress, triggering a debris flow that traveled approximately 2.3 km southward.

The depositional area has a gentle slope gradient. Andesite boulders transported by the debris flow range in size from approximately 0.02 $m^3$ to 4 $m^3$. The depositional area measures about 500 m in length and 250 m in width. In the numerical simulation, the debris-flow area was represented based on contour data using fixed-boundary particles. A scale of 1:3,000 was applied in reconstructing the debris-flow area (Figure 6). The results of the debris-flow modeling were overlaid with satellite imagery to compare the simulated and actual debris-flow distributions, providing a better understanding of the event (Elkarmoty et al., 2017; Vasquez and Estrada, 2023).

The particle radius used for the fixed-boundary particles was set equal to that of the debris-flow particles, with a particle spacing of 7.5 mm. The total number of fixed-boundary and debris-flow particles was 1,582,565. The numerical simulations were performed for 800 seconds to capture the main movement of the debris flow following the collapse of the natural dam. Each simulation iteration used a time step of 1 second. The modeled concentration value was set to 0.3, following Sadisun et al. (2019), who reported that this viscosity value was most representative of the Pasir Panjang debris flow event on February 22, 2018. All parameters used in the numerical simulation are listed in Table 2.

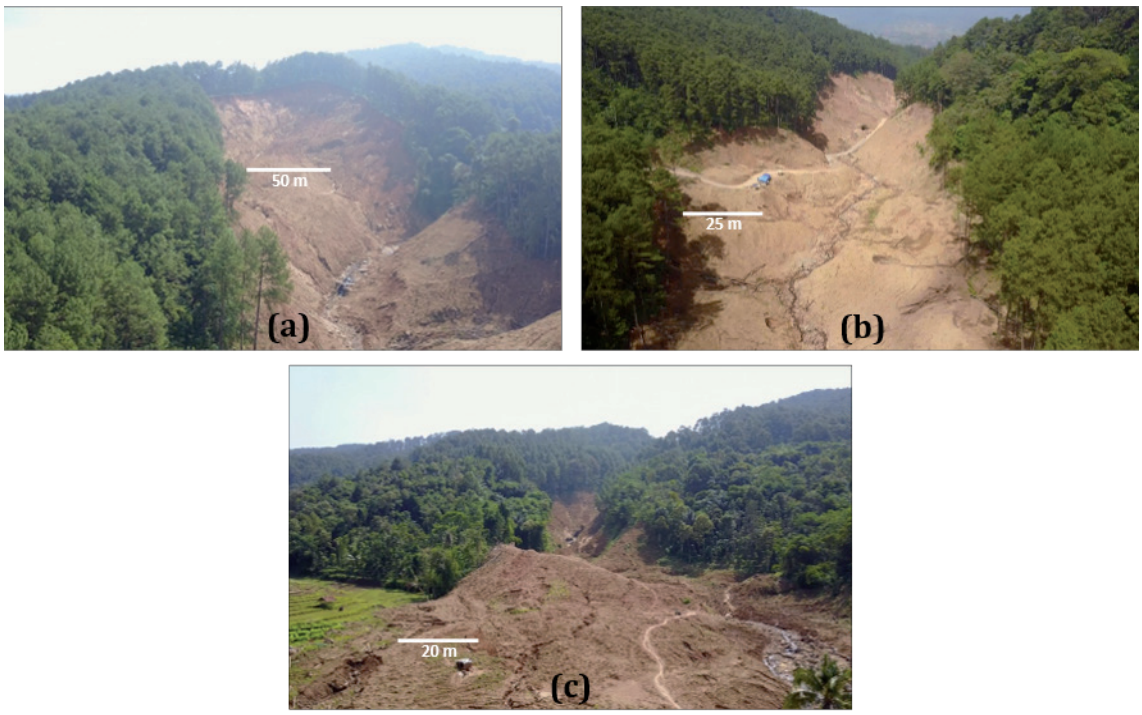


**Figure 5.** (a) Landslide geometry as seen from the south of the source area, (b) river geometry forming the flow track, and (c) condition of debris material in the depositional area.

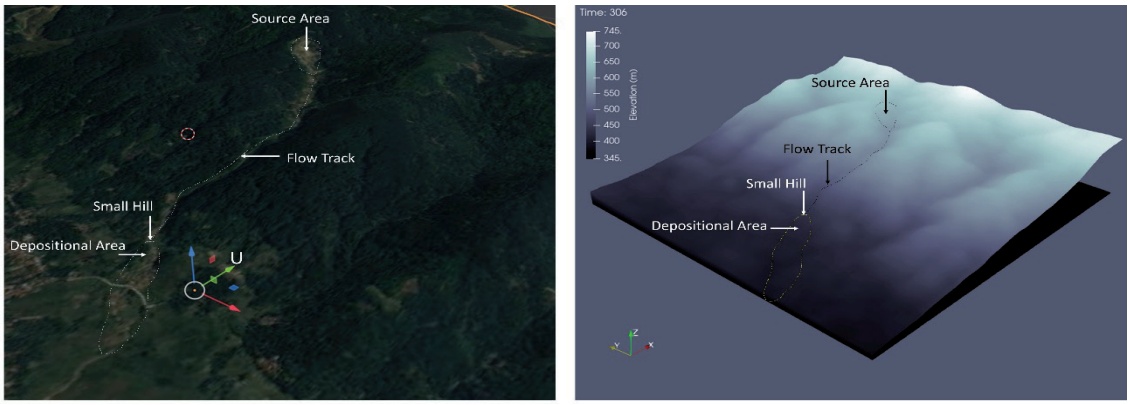


**Fig. 4.** Satellite image of debris flow traces of the Pasir Panjang Debris Flow on February 22, 2018 (left) and the results of the debris flow area reconstruction in SPH (right)

**Figure 6.** (left) Satellite image of debris flow traces of the Pasir Panjang Debris Flow on February 22, 2018 and (right) the results of the debris flow area reconstruction in SPH.

**Table 2.** Parameter values used in numerical simulations

| Parameter | Value | Unit |
|---|---|---|
| Simulation duration | 800 | second |
| Time step calculation | 1 | second |
| Concertation | 0,3 | - |
| Minimum flow density | 700 | $kg/m^3$ |
| Maximum flow density | 1,500 | $kg/m^3$ |
| Water density | 1,000 | $kg/m^3$ |
| Solid material density | 2,607 | $kg/m^3$ |
| Gravity | 9.81 | $m/s^2$ |
| Sound speed coefficient | 20 | - |
| Smooth length coefficient | 1.2 | - |
| Particle distance | 7.5 | mm |
| Cohesion | 20 | kPa |
| Internal friction angle | 23 | ° |
| π | 22/7 | - |

## 5. Results

The numerical simulation results indicate that the debris-flow event initiated with the collapse of the natural dam at t = 1 s, when debris material began to move southeastward along the flow path (Figure 7). The natural dam had a maximum thickness of approximately 8.8 m. At t = 30 s, the debris flow reached the area immediately north of the bridge with a velocity of about 2.5 m/s (Figure 8). The bridge was destroyed at t = 40 s under an estimated impact pressure of 100 kPa, after which the flow deflected southward, following the existing river channel. By t = 120 s, the flow velocity increased to approximately 6 m/s within the confined section of the flow track, attributed to the progressively narrower and straighter channel geometry (Figure 9).

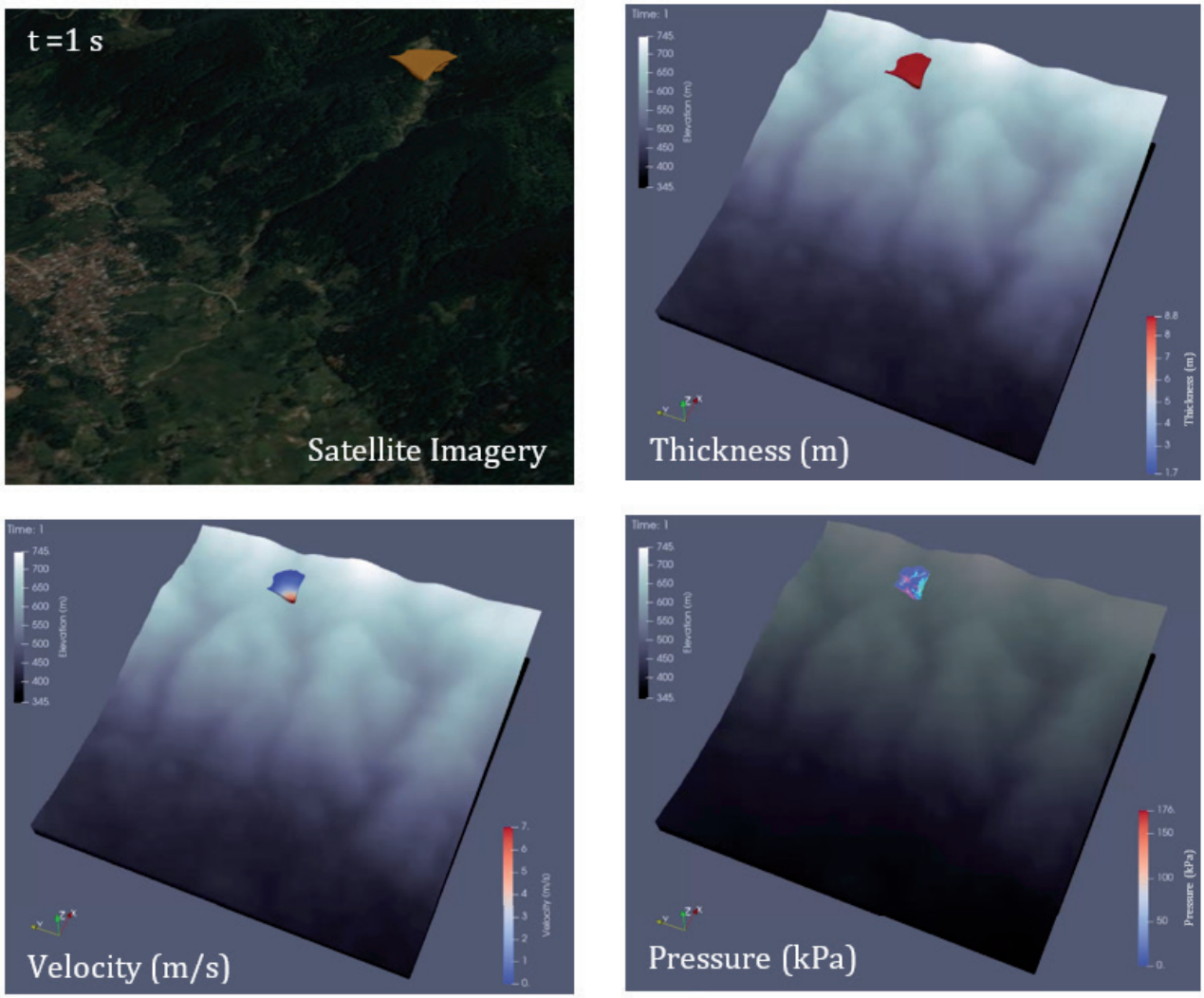


**Figure 7.** Results of numerical simulation of debris flow from the source area to the flow track at t = 1 s.

At t = 130 s, the debris flow impacted a small hill located north of the depositional area, producing a maximum flow thickness of approximately 4 m and an impact pressure of about 30 kPa (Figure 10). A total of 18 individuals were affected by the debris flow in this area while conducting agricultural activities in nearby rice fields. Based on the simulation results, the warning or reaction time available before impact was approximately 10 seconds, determined from the moment the debris flow was first visible from the top of the hill (t = 120 s) to the moment of impact (t = 130 s). This short response window likely contributed to the inability of those in the area to evacuate in time.

The debris flow began to enter the deposition area at t = 150 s forming an alluvial fan (Figure 11). The debris flow began to turn southeast following the river flow direction at t=210 s (Figure 12). The debris flow material began to spread widely and settle in the deposition area at t = 420 s, forming deposits with an approximate thickness of 2 m (Figure 13). By t = 800 s the debris flow continued to flow to the southeast, although the flow thickness gradually decreases as the material further dispersed downstream (Figure 14).

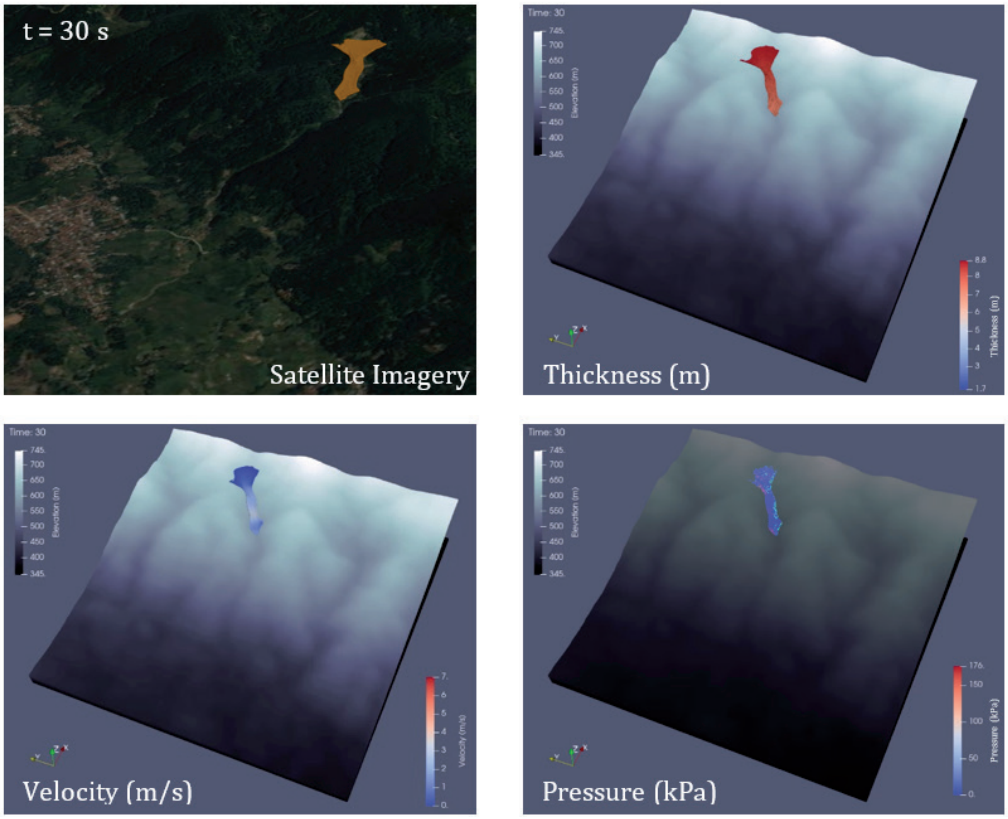


**Figure 8.** Results of numerical simulation of debris flow from the source area to the flow track at t= 30 s.

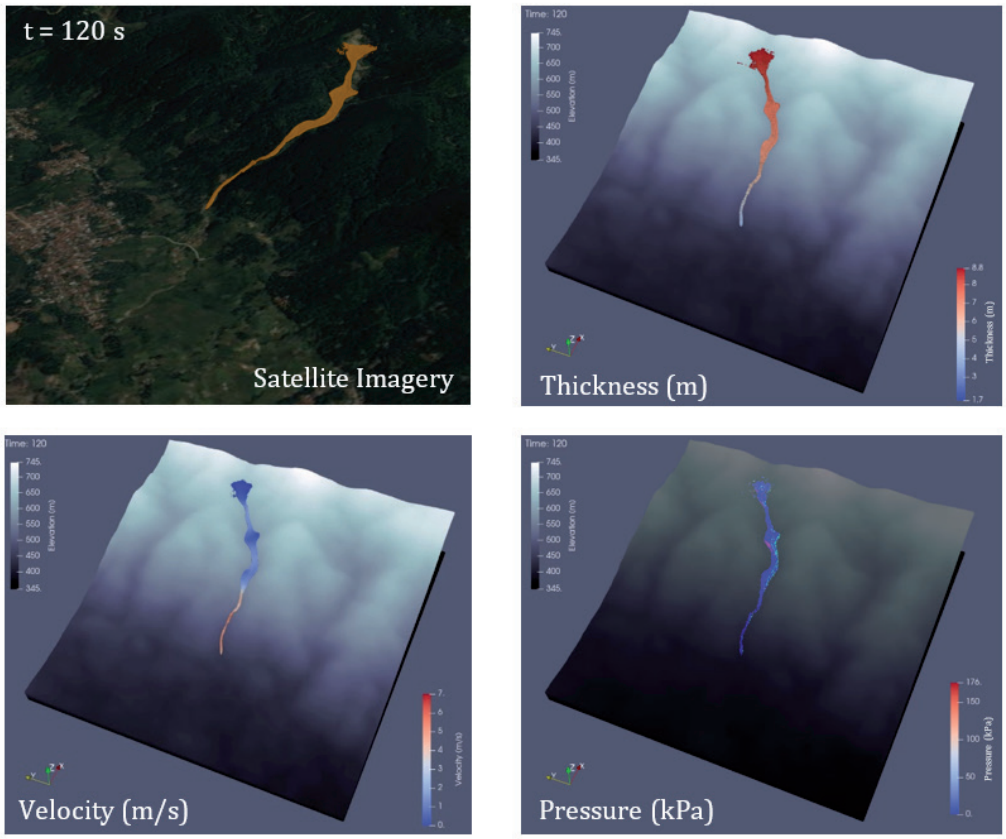


**Figure 9.** Results of numerical simulation of debris flow from the source area to the flow track at t =120 s.

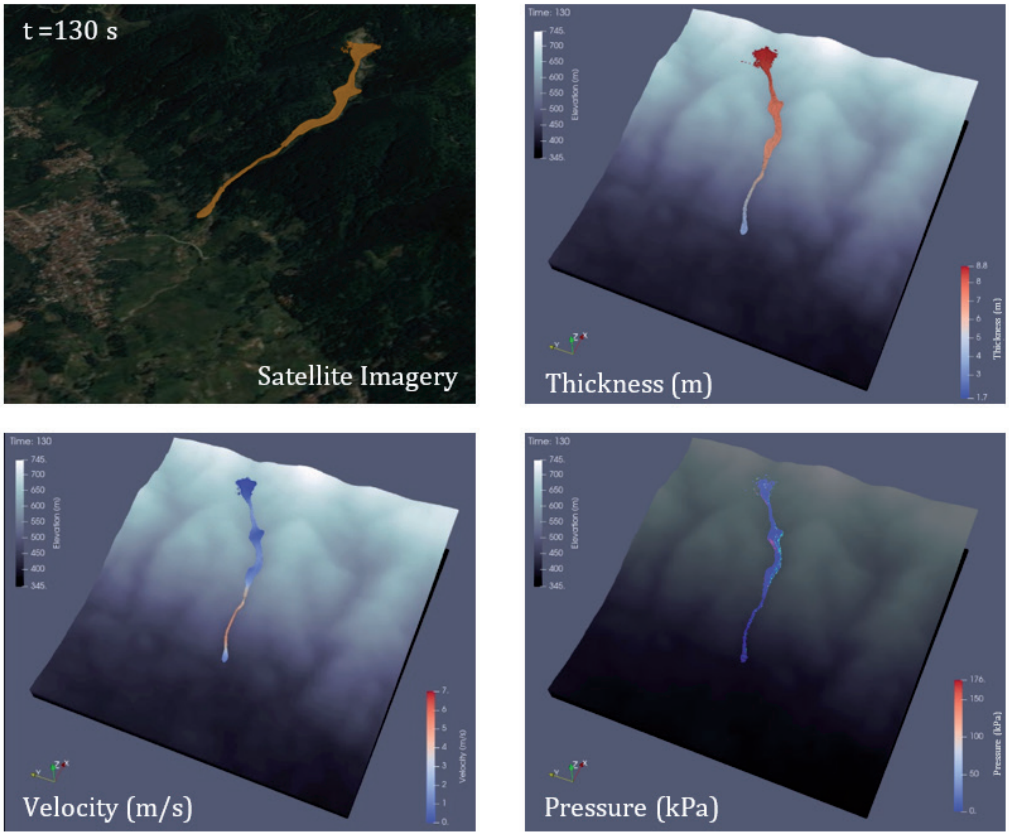


**Figure 10.** Results of numerical simulation of debris flow from the source area to the flow track at t = 130 s.

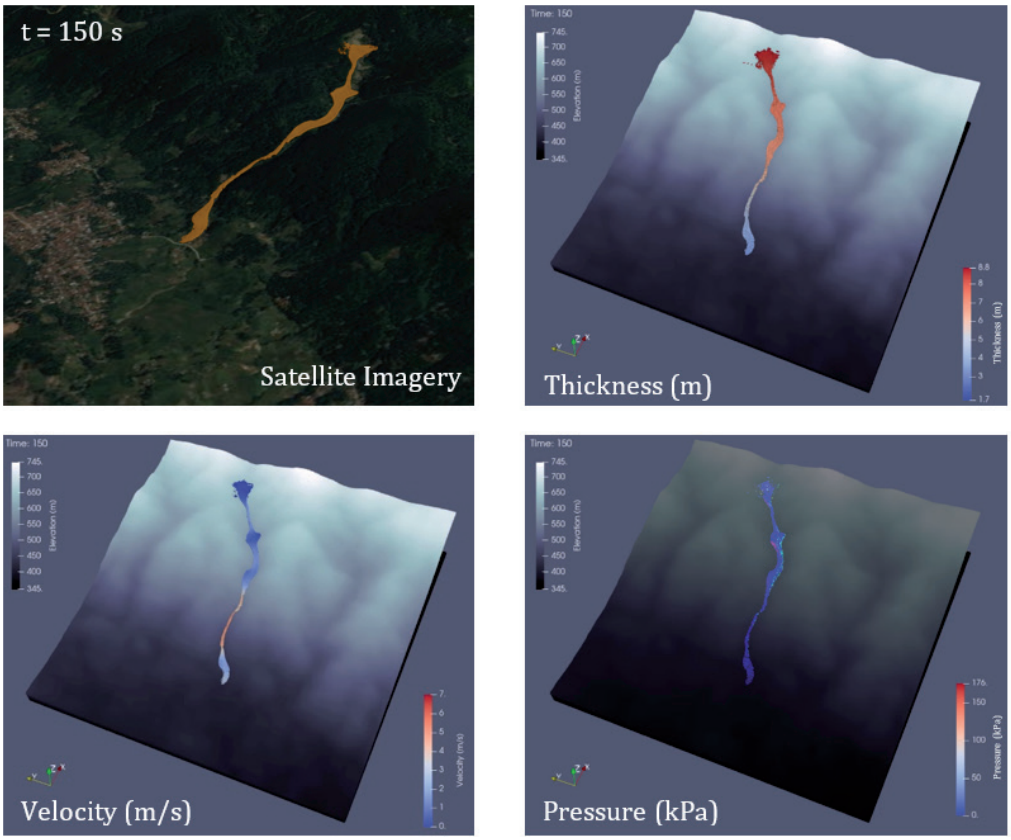


**Figure 11.** Results of numerical simulation of debris flow in the depositional area at t = 150 s.

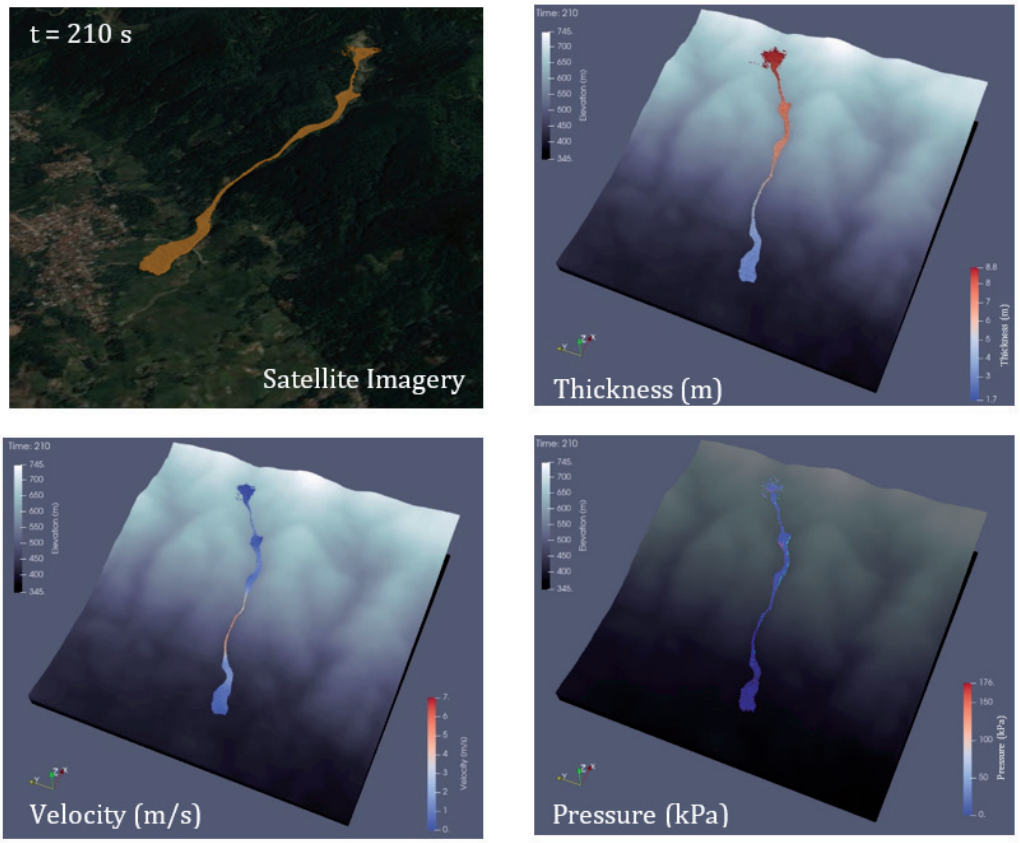


**Figure 12.** Results of numerical simulation of debris flow in the depositional area at t = 210 s.

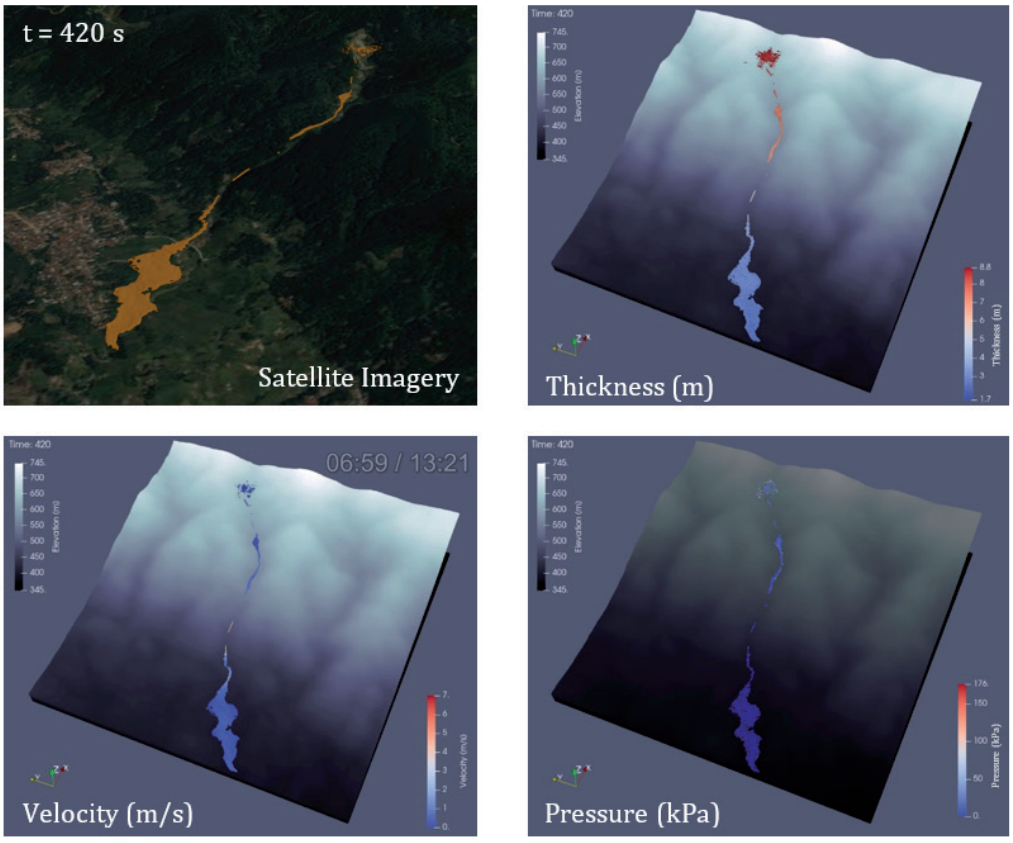


**Figure 13.** Results of numerical simulation of debris flow in the depositional area at t = 420 s.

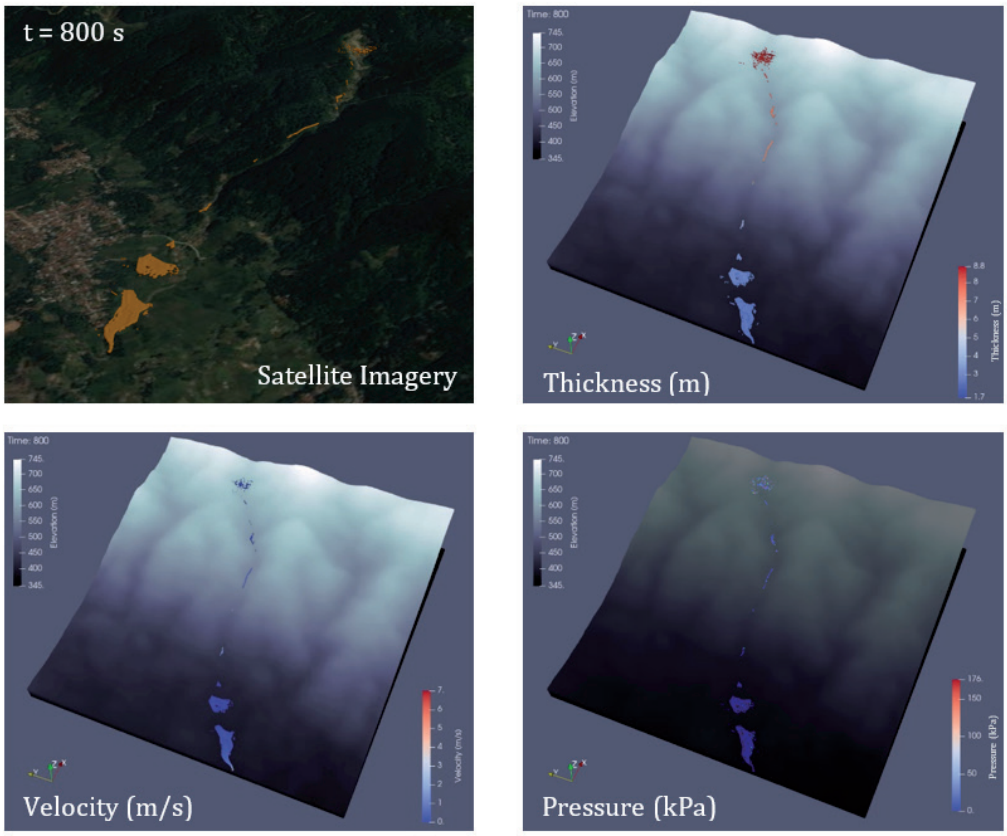


**Figure 14.** Results of numerical simulation of debris flow in the depositional area at t =800 s.

## 6. Discussion

Due to the absence of velocity, thickness, and monitoring data for the Pasir Panjang debris flow event, the comparison between modeling results and the actual event was conducted based on the observed impacts of the debris flow. These impacts include eroded river cliff faces, material deposited after the debris flow occurred, and infrastructure damage (roads and bridges). The modeling parameters analyzed in this study comprise the average velocity, average pressure, and average thickness. The use of average values was performed to simplify the complexity of the modeling output parameters. The SPH-based-debris flow modeling is capable to model the debris flow segregation process, so the details of each output parameter are more complex due to the spatial and temporal conditions. Therefore, a detailed study of the output parameters is beyond the scope of this study.

The average velocity of debris flow modeling showed relatively transverse pattern until t = 126 s (Figure 15). The relatively transverse average velocity pattern was caused by moving debris material not yet aligned in single direction (Gotoh et al., 2002); there were still many modeled particles moving perpendicular to the direction of surface water flow. Between t = 126 s and t = 289 s, the average velocity pattern remained relatively constant, as the modeled particles had become more uniformly oriented, forming a characteristic flow structure and beginning to spread within the depositional area. Between $t$ = 289 s and $t$ = 800 s, the average velocity pattern became more irregular, caused by the fragmentation of the debris-flow body into several parts that continued moving from the flow track toward the depositional area.

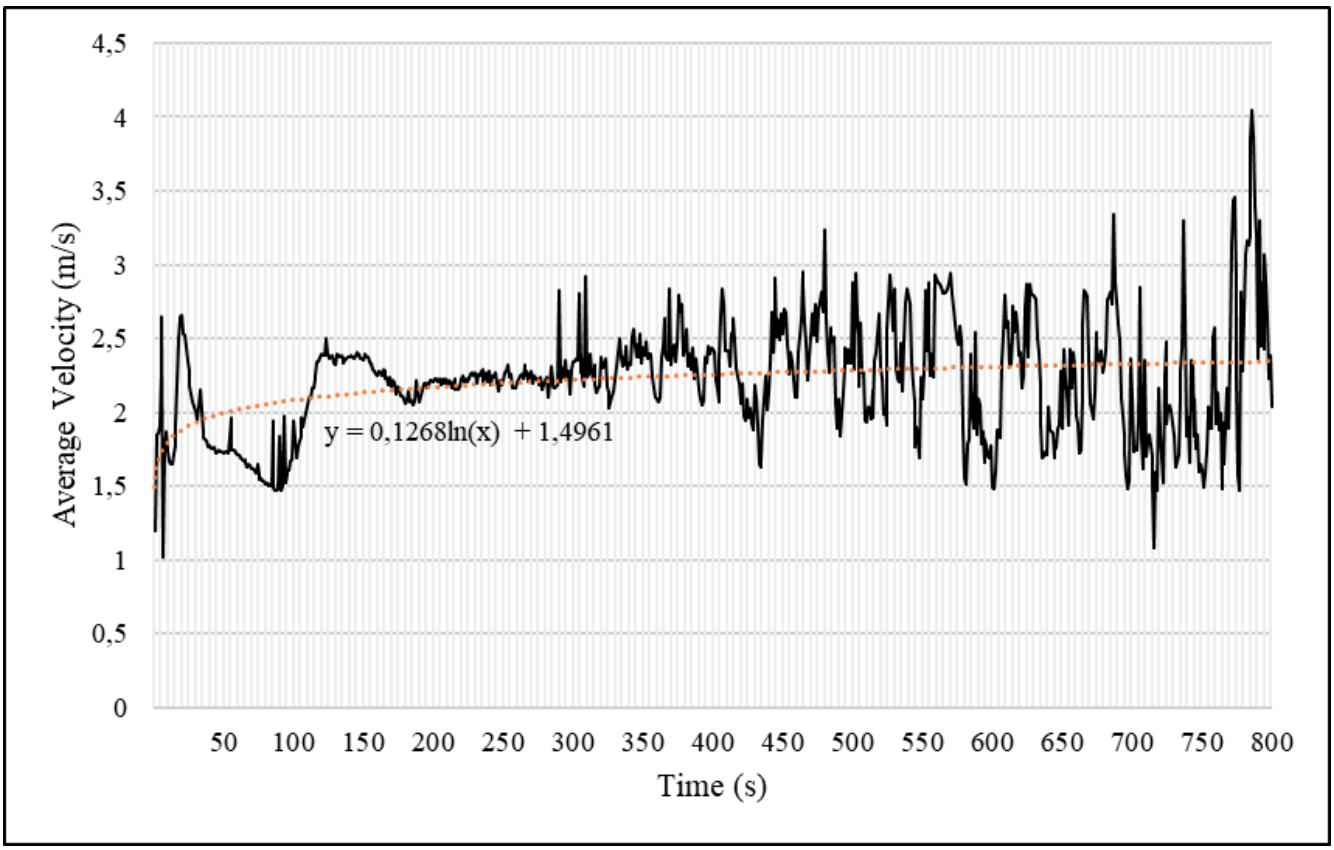


**Figure 15.** Relationship between average velocity and modeling time.

The average pressure graph of the debris-flow simulation exhibited a steep negative gradient from $t$ = 1 s to $t$ = 47 s (Figure 16). This trend reflects the time required for the debris flow to move from the broad source area into the narrow section of the flow track, resulting in a rapid and significant pressure drop. After $t$ = 47 s, the negative gradient became relatively stable, indicating that the average pressure of the debris material was evenly distributed as the flow entered the channelized section with a more defined flow structure. When the debris flow reached the depositional area at $t$ = 150 s, the pressure variation became less significant, as the pressure distribution corresponded to the expansion of the depositional area.

Figure 17 shows the average debris-flow thickness over time. The average thickness exhibited a steep negative gradient from $t$ = 1 s to $t$ = 13 s, corresponding to the time required for the natural dam to completely collapse. Subsequently, the negative gradient became more gradual from $t$ = 13 s to $t$ = 300 s, indicating that the debris material was becoming more evenly distributed as it entered the flow track.

The natural dam collapse process is also indicated by a significant pressure drop and velocity fluctuations between $t$ = 1 s and $t$ = 13 s. The rapid pressure drop resulted from the model's rapid time-step adjustment as it sought to reach a new equilibrium state. Such behavior typically occurs when a retaining mass experiences high pressure leading to failure, as in the collapse of a natural dam. The observed velocity fluctuations reflect transient flow behavior, during which the time-step model continuously adjusted to a changing equilibrium state. In this case, the velocity gradually stabilized after an initial rapid change, corresponding to the period of significant pressure reduction. During this stage, the model had not yet reached equilibrium, causing the velocity to oscillate temporarily before stabilization.

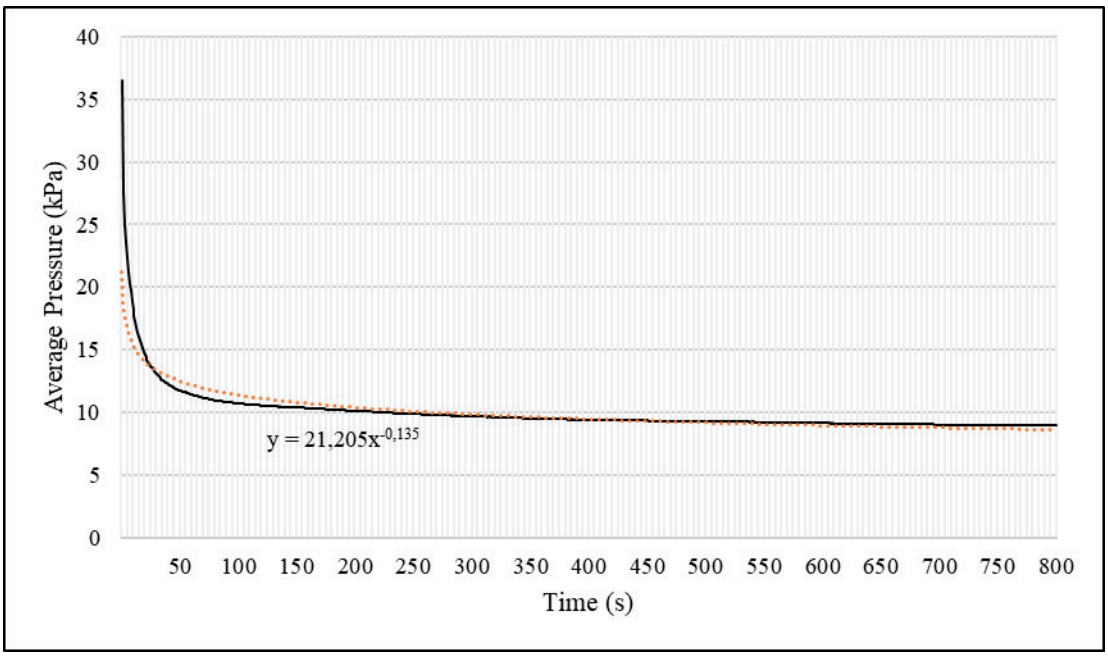


**Figure 16.** Relationship between average pressure and modeling time.

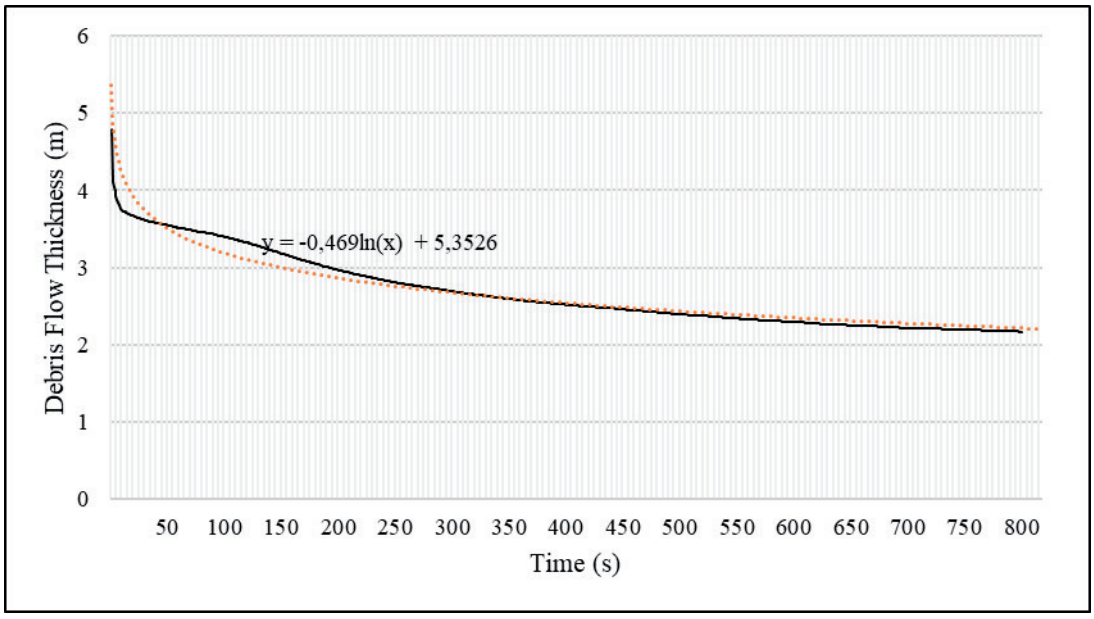


**Figure 17.** Relationship between debris flow thickness and modeling time.

## 7. Conclusions

The governing equations of the flow consist of the continuity and momentum equations in Lagrangian form, developed from various references to accommodate the movement of solid materials, non-Newtonian flow behavior, and interactions between solid and liquid particles. The numerical simulation in this study employed the smoothed particle hydrodynamics (SPH) method using a 1:3,000 scale model. The debris-flow modeling time was 800 s with a 1-s time step, resulting in a total of 1.2 billion modeled particles and an ideal processing time of approximately 36 hours. The simulation results showed that the collapse of the natural dam began at $t$ = 1 s, with debris material entering the flow track at a maximum thickness of 8.8 m. The bridge was destroyed at $t$ = 40 s under a pressure of 100 kPa. A velocity of 6 m/s was reached at $t$ = 120 s within the flow track. At $t$ = 130 s, a small hill north of the depositional area was struck by the debris flow, with a thickness of 4 m and pressure of 30 kPa, resulting in 18 fatalities. The debris flow entered the depositional area at $t$ = 150 s, forming an alluvial fan, and began to spread and settle by $t$ = 420 s, with an average thickness of approximately 2 m.

The average velocity of the debris-flow model exhibited a relatively transverse pattern from $t$ = 1 s to $t$ = 126 s, caused by the debris material not yet being fully oriented in one flow direction. From $t$ = 126 s to $t$ = 289 s, the average velocity remained relatively constant as the modeled particles began moving uniformly with a typical flow shape and started to spread within the depositional area. Between $t$ = 289 s and $t$ = 800 s, the average velocity became irregular due to the debris-flow body fragmenting into several parts that continued moving from the flow track toward the depositional area.

The average pressure of the debris-flow model exhibited a steep negative gradient from $t$ = 1 s to $t$ = 47 s, caused by the time required for the debris flow to move from a wide source area into a narrow section of the flow track. After $t$ = 47 s, the negative gradient became relatively flat, indicating that the average pressure of the debris material was evenly distributed as it began to enter the flow track with a typical flow shape. Similarly, the average debris-flow thickness showed a steep negative gradient from $t$ = 1 s to $t$ = 13 s, corresponding to the time required for the natural dam to completely collapse. The gradient then became gentler from $t$ = 13 s to $t$ = 800 s, indicating that the debris material was gradually and evenly distributed as it entered the flow track.

This research is limited to modeling debris flows in its granular form, without accounting for changes in debris volume from erosion or deposition. Future studies will focus on analyzing the volume changes from erosion and deposition in greater details and investigating relationship between key parameters and their spatial and temporal variations.

## Acknowledgments

The authors would like to acknowledge the financial support provided by ITB research grant, Bandung Institute of Technology, which collectively funded this research.

## References

Agostino, V. D., Tecca, P. R., 2006. Some considerations on the application of the FLO-2D model for debris flow hazard assessment. WIT Transactions on Ecology and the Environment 90, 159-170, https://doi.org/10.2495/DEB060161

Ahmid, D. A., Wahyudi, T., Kusnawan, Gunawan, Zulfahmi, Supriyanto, B. A., Cahyono, S. S., Tarsono, Setiawan, L., 2023. Landslide potential in Cihanjuang, Cimanggung, Sumedang, West Java Province. Jurnal Riset Geologi dan Pertambangan 33, 89–97, https://doi.org/10.55981/risetgeotam.2023.1228

Alvioli, M., Baum, R. L., 2016. Parallelization of the TRIGRS model for rainfall-induced landslides using the message passing interface. Environmental Modelling & Software 81, 122-135, https://doi.org/10.1016/j.envsoft.2016.04.002

Berger, C., Schlunnegger, F., McArdell, B. W., 2011. Direct measurement of channel erosion by debris flows, Illgraben, Switzerland. Journal of Geophysical Research 116, 1-18, https://doi.org/10.1029/2010JF001722

Blijenberg, H. M., 2007. Application of physical modelling of debris flow triggering to field conditions: limitations posed by boundary conditions. Engineering Geology 91, 25-33, https://doi.org/10.1016/j.enggeo.2006.12.010

Canelas, R. B., Dominguez, J. M., Crespo, A. J. C., Gomez-Gesteira, M., Ferreira, R. M. L., 2017. Resolved Simulation of a Granular-Fluid Flow with a Coupled SPH-DCDEM Model, Journal of Hydraulic Engineering 143, 1-22, https://doi.org/10.1061/(ASCE)HY.1943-7900.0001331

Choi, C. E., Au-Yeung, S. C. H., Ng, C. W. W., Song, D., 2015. Flume investigation of landslide granular debris and water runup mechanisms, Géotechnique Letters 5, 28–32, https://doi.org/10.1680/geolett.14.00080

Choi, C. E., Goodwin, G. R., Ng, C. W. W., Cheung, D. K. H., Kwan, J. S. H., Pum, W. K., 2016. Coarse granular flow interaction with slit structures. Géotechnique Letters 6, 1–8, https://doi.org/10.1680/jgele.16.00103

Domínguez, J. M., Fourtakas, G., Altomare, C., Canelas, R. B., Tafuni, A., García-Feal, O., Estévez, I. M., Mokos, A., Vacondio, R., Crespo, A. J. C., Rogers, B. D., Stansby, P. K., Gesteira, M. G., 2021. State-of-the-art SPH solver DualSPHysics: from fluid dynamics to multiphysics problems. Computational Particle Mechanics 9, 867-895, https://doi.org/10.48550/arXiv.2104.00537

Dzaki, M. F., Setiawan, H., Hidayat, R., 2024. Landslide susceptibility zonation using weight of evidence method in Mertelu and Tegalrejo, Gedangsari, Gunungkidul, Special Region of Yogyakarta, Indonesia. Jurnal Riset Geologi dan Pertambangan 34, 67-82, https://doi.org/10.55981/risetgeotam.2024.1299

Elkarmoty, M., Colla, C., Gabrielli, E., Kasmaeeyazdi, S., Tinti, F., Bondua, S., Bruno, R., 2017. Mapping and modelling fractures using ground penetrating radar for ornamental stone assessment and recovery optimization: Two case studies. Rudarsko-geološko--naftni zbornik 32(4), 63-76, https://doi.org/10.17794/rgn.2017.4.7

Federico, F., Cesali, C., 2019. Effects of granular collisions on the rapid coarse-grained materials flow. Géotechnique Letters 9, 1–6, https://doi.org/10.1680/jgele.18.00223

Fourtakas, G., Rogers, B. D., 2016. Modelling multi-phase liquid-sediment scour and resuspension induced by rapid flows using Smoothed Particle Hydrodynamics (SPH) accelerated with a Graphics Processing Unit (GPU). Advances in Water Resource 92, 186–199, https://doi.org/10.1016/j.advwatres.2016.04.009

Gotoh, T., Fukayama, D., Nakano, T., 2002. Velocity field statistics in homogeneous steady turbulence obtained using a high-resolution direct numerical simulation. Physics of Fluids 14, 1065-1081, https://doi.org/10.1063/1.1448296

Hsu, Y., Liu, K., 2019. Combining TRIGRS and DEBRIS-2D models for the simulation of a rainfall infiltration induced shallow landslide and subsequent debris flow. Water 11, 890, https://doi.org/10.3390/w11050890

Hussin, H. Y., Luna, B. Q., van Westen, C. J., Christen, M., Malet, J. P., van Asch, T. W. J., 2012. Parameterization of a numerical 2-D debris flow model with entrainment: a case study of the Faucon catchment, Southern French Alps. Nat. Hazards Earth Syst. Sci. 12, 3075–3090, https://doi.org/10.5194/nhess-12-3075-2012

Jakob, M, 2010. State of the art in debris-flow research: the role of dendrochronology, 183-232 in Stoffen, M., Bollschweiler, M., Butler, D. R., Luckman, B. H., ed., Tree Rings and Natural Hazards. Springer.

Jakob, M., Hungr, O., 2005. Debris-flow Hazard and Related Phenomena. Praxis Publishing Ltd.

Janda, R. J., Scott, K. M., Nolan, K. M., Martinson, H. A., 1981. Lahar movement, effects, and deposits. United States Government Printing Office.

Jiang, Y. J., Zhao, Y., 2015. Experimental investigation of dry granular flow impact via both normal and tangential force measurements. Géotechnique Letters 5, 33–38, https://doi.org/10.1680/geolett.15.00003

Kastowo, 1975. Regional Geological Map of Majenang Quadrangle, Java, Scale1:100,000. Geological Agency of Indonesia.

Lo, Y. M. E., Shao, S., 2002. Simulation of near-shore solitary wave mechanics by an incompressible SPH method. Applied Ocean Research 24, 275-286, https://doi.org/10.1016/S0141-1187(03)00002-6

Mitsoulis, E., 2007. Flows of viscoplastic materials: Models and computations. The British Society of Rheology.

Monaghan, J. J., 1992. Smoothed Particle Hydrodinamics. Annu. Rev. Astron. Astrophys. 30, 543-574, https://doi.org/10.1146/annurev.aa.30.090192.002551

Monaghan, J. J., 1994. Simulating Free Surface Flows with SPH. Journal of Computational Physics 110, 399–406, https://doi.org/10.1006/jcph.1994.1034

Monaghan, J. J., Kos, A., Issa, N., 2003. Fluid motion generated by impact. Journal of Waterway, Port, Coastal, Ocean Engineering 129, 250-259, https://doi.org/10.1061/(ASCE)0733-950X(2003)129:6(250)

Morris, J. P., Fox, P. J., Zhu, Y., 1997. Modeling Low Reynolds Number Incompressible Flows Using SPH. Journal of Computational Physics 130, 214-226, https://doi.org/10.1006/jcph.1997.5776

Nettleton, I. M., Martin, S., Hencher, S., Moore, R., 2005. Debris flow types and mechanisms. The Scottish Executive.

Papanastasiou, T. C., 1987. Flows of Materials with Yield. Journal of Rheology 31, 385–404, https://doi.org/10.1122/1.549926

Pierson, T. C., 1980. Erosion and deposition by debris flows at Mount Thomas, North Canterbury, New Zealand. Earth Surface Process 5, 227-247, https://doi.org/10.1002/esp.3760050302

Putra, M. H. Z., Dinata, I. A., Sadisun, I. A., Sarah, D., Aulia, A. N., Sukristiyanti, 2022. Modeling of individual debris flows based on DEMNAS using Flow-R: A case study in Sigi, Central Sulawesi. Jurnal Riset Geologi dan Pertambangan 32, 37-58, https://doi.org/10.14203/risetgeotam2022.v32.1215

Sadisun, I. A., Kartiko, R. D., Dinata, I. A., 2018. Numerical Simulation of Some Debris Flow Events in Central Java for Predicting Run-out Distributions. Proceedings of SEAGS-AGSSEA Conference 2018, 357-360, Jakarta, Indonesia.

Sadisun, I. A., Dinata, I.A., Kartiko, R. D., 2019. Run-out Distribution of Pasir Panjang Landslides Followed by the Debris Flow, Central Java, Indonesia. IAEG ARC12 2019, Jeju, South Korea.

Song, D., Choi, C. E., Zhou, G. G. D., Kwan, J. S. H., Sze, H. Y., 2018. Impulse Load Characteristics of Bouldery Debris Flow Impact. Géotechnique Letters 8, 111–117, https://doi.org/10.1680/jgele.17.00159

Vasquez, J., Estrada, M., 2023. A comparative study of the bivariate statistical methods and the Analytical Hierarchical Process for the assessment of mass movement susceptibility. A case study: The LM-116 Road – Peru. Rudarsko-geološko-naftni zbornik 38(62), 149-166, https://doi.org/ 10.17794/rgn.2023.1.13